High-Resolution Structure and Mechanism of an F/V-Hybrid Rotor Ring in a Na^+-coupled ATP Synthase

SUPPLEMENTARY INFORMATION

Doreen Matthies[1#], Wenchang Zhou[2#], Adriana L. Klyszejko[1§], Claudio Anselmi[2§], Özkan Yildiz[1], Karsten Brandt[3], Volker Müller[3], José D. Faraldo-Gómez[2,4]* and Thomas Meier[1,4]*

[1]*Department of Structural Biology, Max Planck Institute of Biophysics, Max-von-Laue-Strasse 3, 60438 Frankfurt am Main, Germany*

[2]*Theoretical Molecular Biophysics Section, National Heart, Lung & Blood Institute, National Institutes of Health, Bethesda, MD 20892, USA*

[3]*Molecular Microbiology & Bioenergetics, Institute of Molecular Biosciences, Goethe-University Frankfurt, Max-von-Laue-Strasse 9, 60438 Frankfurt am Main, Germany*

[4]*Cluster of Excellence Macromolecular Complexes, Goethe-University Frankfurt, Max-von-Laue-Strasse 15, 60438 Frankfurt am Main, Germany*

[#]*These authors contributed equally*

[§]*These authors contributed equally*

**Corresponding authors:*
TM: thomas.meier@biophys.mpg.de
JDFG: jose.faraldo@nih.gov

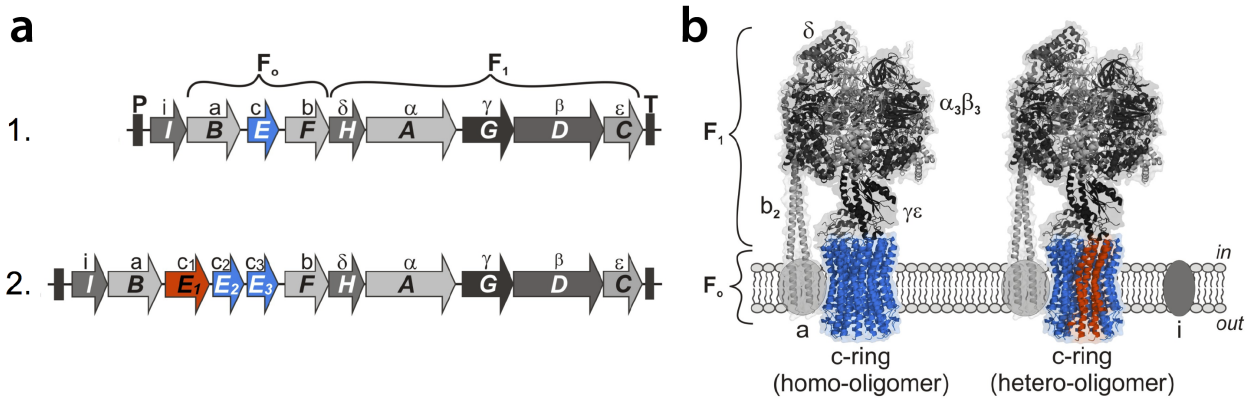

Supplementary Figure 1. Organization of the *atp*-operon coding for the *Acetobacterium woodii* F_1F_o ATP synthase, and overall enzyme architecture. (**a**) Typical bacterial *atp*-operons (1) contain nine genes (*atpIBEFHAGDC*), only one of which codes for the single-hairpin c-subunit that forms c-rings in the membrane. In contrast, *Acetobacterium woodii* is one among several organisms[§] whose *atp*-operon features multiple genes coding for different c-subunits (2). Subunits c_2 and c_3 are single-hairpin c-subunits identical to each other in their amino acid sequence. The c_1 subunit is, however, more similar to the double-hairpin c-subunits of V-type ATPases or A-type ATP synthases[§]. **(b)** Hypothetical mosaic models of the bacterial F_1F_o-ATP synthase, highlighting the membrane-embedded c-ring in blue. The V-like c_1 subunit in the *A. woodii* ring is highlighted in orange. The models were generated by combining PDB entries 1YCE, 1B9U, 3K5B, 2A7U, 2QE7 and 1E79. Subunit-a and the *atpI* gene product, whose structures are unknown, are indicated by ellipsoids. Subunits $\alpha_3\beta_3$ form the catalytic domain, which is in the cytoplasm. This assembly is mechanically coupled to the c-ring via subunits γ and ε, referred to as the central stalk. The peripheral stalk, which consists of a subunit-b dimer and subunit-δ, bridges the $\alpha_3\beta_3$ headpiece with subunit-a, in the membrane. In the operating enzyme, only the c-ring and the central stalk rotate, concertedly. Counter-clockwise rotation (viewed from F_1) is associated with inward ion translocation across the interface between the c-ring and subunit-a, and with ATP synthesis/release in/from $\alpha_3\beta_3$. Clockwise rotation is instead associated with outward ion translocation and ATP hydrolysis. These competing processes are known to involve large conformational changes within the $\alpha_3\beta_3$ headpiece; changes within subunit-a have been also proposed.

[§]Matthies D. Biochemical and structural analysis of F-type ATP synthases and its subcomplexes. Doctoral dissertation. Johann Wolfgang Goethe-University, Frankfurt am Main, Germany (2013).

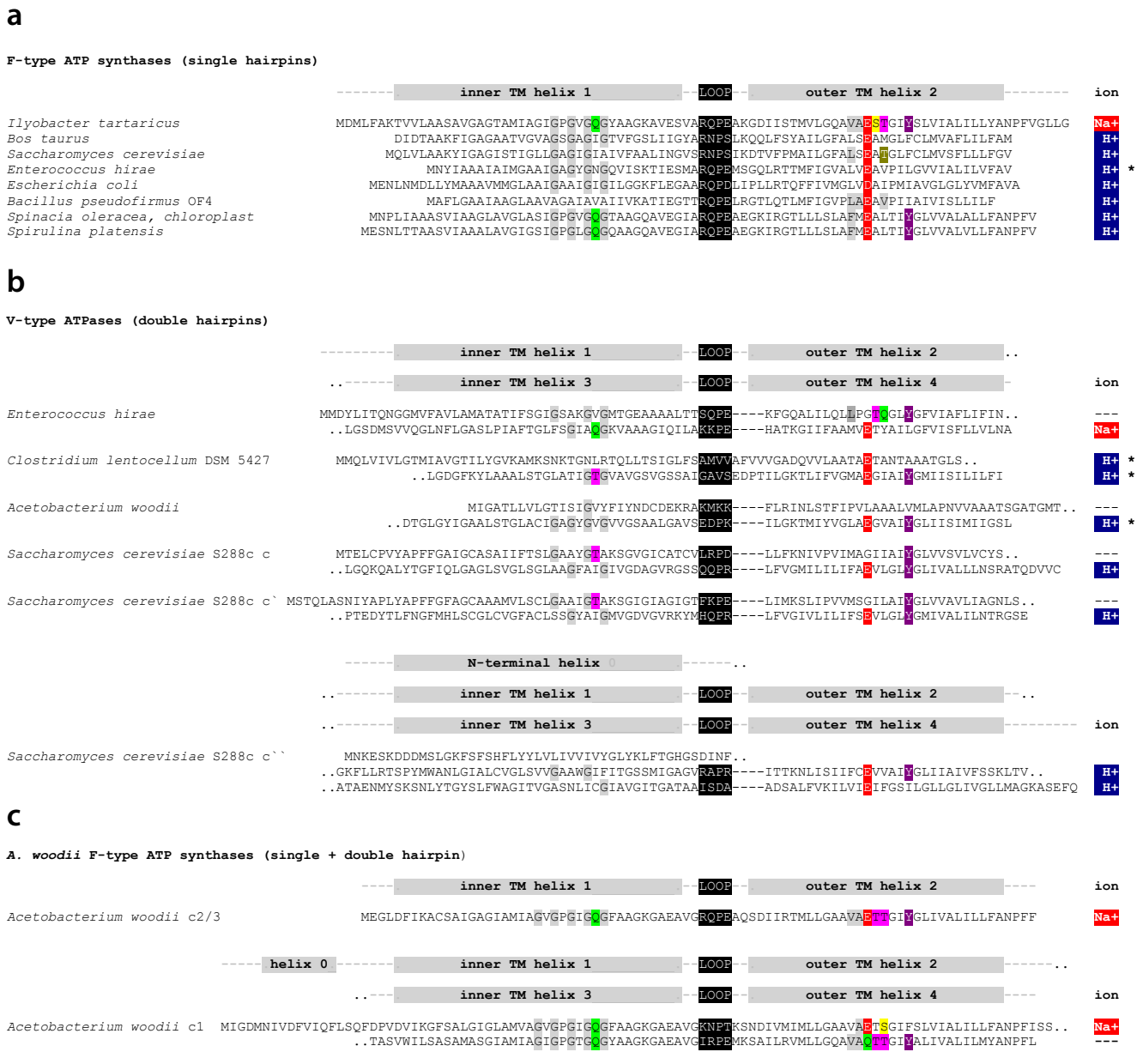

Supplementary Figure 2. Comparison of the sequences and topologies of representative c-subunits. (**a**) Sequences from prototypical single-hairpin c-subunits in F-type ATP synthases. These c-subunits assemble into homomeric c-rings. The approximate transmembrane (TM) region of each of the two α-helices is indicated (gray boxes). (**b**) Sequences from prototypical double-hairpin c-subunits from selected V-type ATPases. Note that some of these c-subunits form heteromeric rings, and that in some cases the c-subunit features an N-terminal extension. (**c**) *Acetobacterium woodii* is one among several organisms[§] whose ATP synthase features two kinds of c-subunits with distinct amino-acid sequence. Residues highlighted in color are either known or predicted to be involved in ion binding. The coupling ion, either known or predicted (*), is indicated in each case.

[§]Matthies D. Biochemical and structural analysis of F-type ATP synthases and its subcomplexes. Doctoral dissertation, Johann Wolfgang Goethe-University, Frankfurt am Main, Germany (2013).

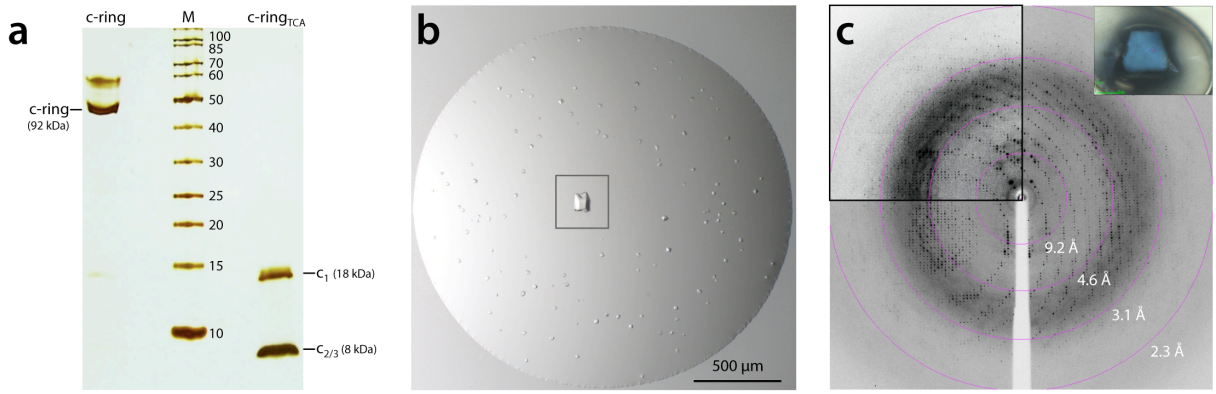

Supplementary Figure 3. Purification and crystallization of the *Acetobacterium woodii* c-ring. (**a**) SDS-PAGE of purified c-ring from wild-type *A. woodii* cells. The ring runs as a stable hetero-oligomer and can be precipitated into its c-monomers by acidification, using trichloroacetic acid (TCA). The ATP synthase was solubilized from membranes and purified by PEG-precipitation. The c-ring was extracted by detergent solubilization, ammonium-sulfate precipitation, anion-exchange chromatography and density-gradient centrifugation. (**b**) Crystallization was accomplished using the vapor-diffusion hanging-drop method, at pH 4.5. (**c**) The crystal shown in the figure diffracted up to a resolution of 2.1 Å.

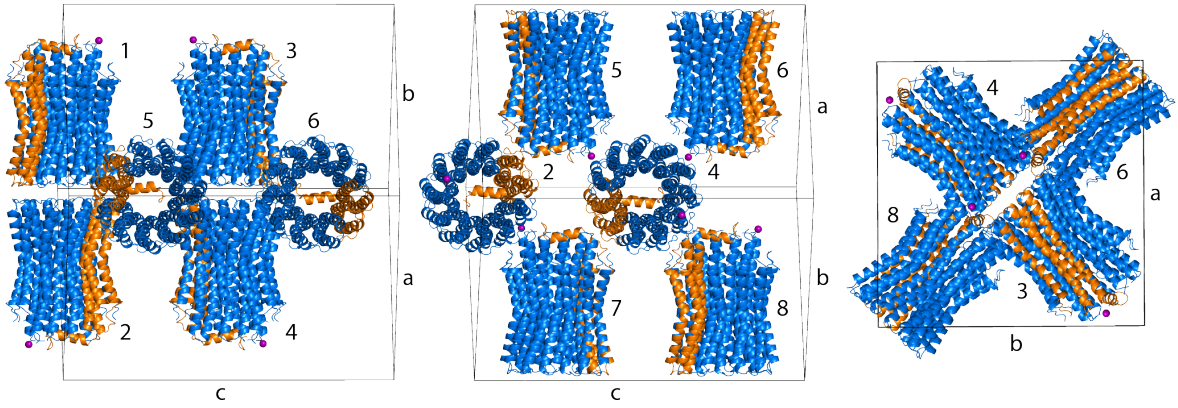

Supplementary Figure 4. Crystal packing of the *A. woodii* c-ring in space group $P4_32_12$. The dimensions of the unit cell are a = b = 121.2 Å and c = 150.6 Å, with $\alpha = \beta = \gamma = 90°$. The unit cell contains eight c-rings (numbered) and the asymmetric unit is one complete c-ring. Subunits $c_{2/3}$ are colored in blue, and subunit c_1 in orange. The lattice contacts involve (i) interactions between most of the cytoplasmic loops in two rings, head to head (for example molecules 1 and 2); (ii) interactions between the N-termini of TM1 in two $c_{2/3}$ subunits of one ring, and the N-terminus of TM4 in the c_1 subunit of another (for example, molecules 2 and 5), and (iii) the N-termini of TM1 in two $c_{2/3}$ subunits of one ring, and the N-termini of TM2 in two $c_{2/3}$ subunit of another (for example, molecules 2 and 7). The latter contact is mediated by a Mn^{2+} ion (purple sphere).

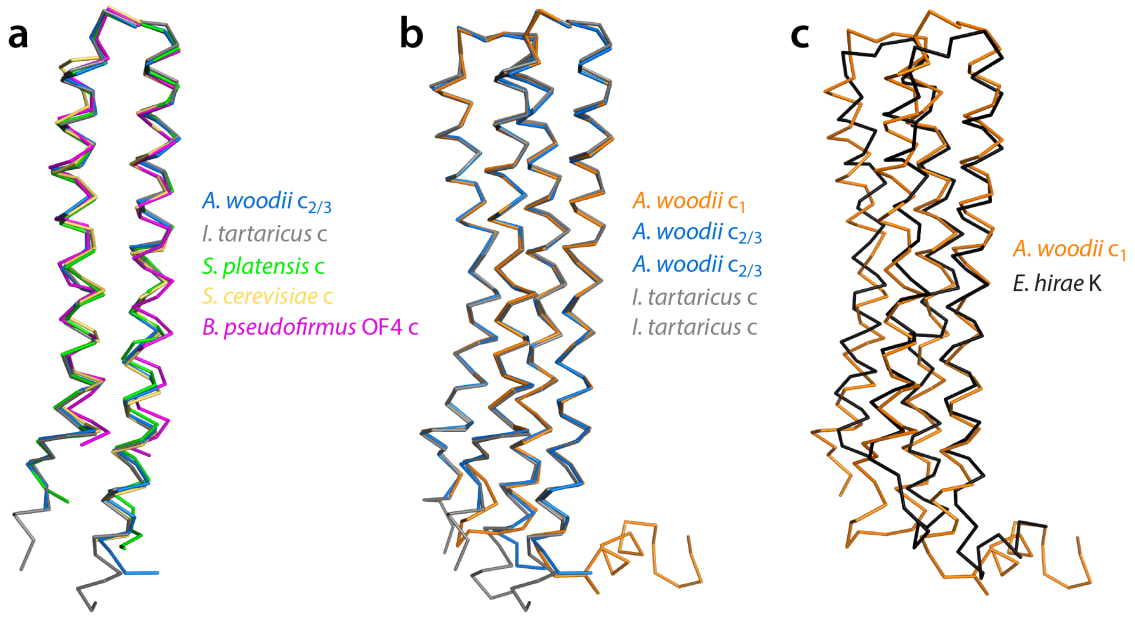

Supplementary Figure 5. Comparison of prototypical F- and V-type c-subunit structures. (**a**) Subunit $c_{2/3}$ from the *A. woodii* ATP synthase is overlaid on the F-type c-subunits from *Ilyobacter tartaricus* (the RMSD for all Cα atoms is 0.39 Å), *Spirulina platensis* (RMSD 0.61 Å) *Saccharomyces cerevisiae* (RMSD 1.08 Å), and *Bacillus pseudofirmus* OF4 (RMSD 1.09 Å). (**b**) The N- and C-terminal hairpins of the c_1 subunit from *A. woodii* (residues 1-102 and 103-182, respectively) are compared with the $c_{2/3}$ subunit from *A. woodii* (RMSD 0.29 and 0.24 Å, respectively) and with the c-subunit from *I. tartaricus* (RMSD 0.46 and 0.45 Å, respectively), each overlaid independently. A similar fit (not shown) is obtained if two adjacent $c_{2/3}$ subunits in the *A. woodii* c-ring, or two adjacent c-subunits in the *I. tartaricus* c-ring, are simultaneously overlaid on the c_1 subunit (RMSD 0.34 and 0.54 Å, respectively). (**c**) A two-hairpin K-subunit from the Na^+-coupled ring of the V-type ATPase from *Enterococcus hirae* is compared with subunit c_1 from *A. woodii* (RMSD 1.85 Å).

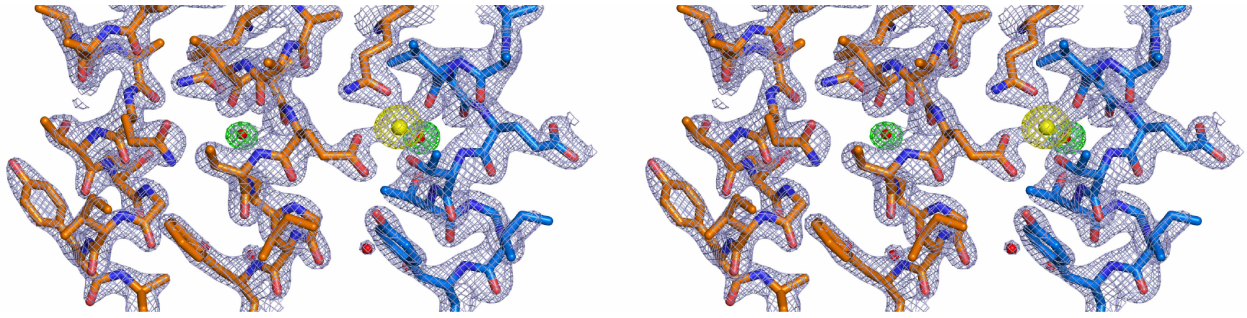

Supplementary Figure 6. Stereo-view of the water-binding site within the c_1 subunit, and the Na^+-binding site at the $c_1/c_{2/3}$ interface. The figure shows F_o-F_c maps calculated for either Na^+ or water molecules (yellow and green mesh, respectively), contoured at +4.0σ. The $2F_o-F_c$ map for the protein is also shown, contoured at 2.4σ (light blue mesh).

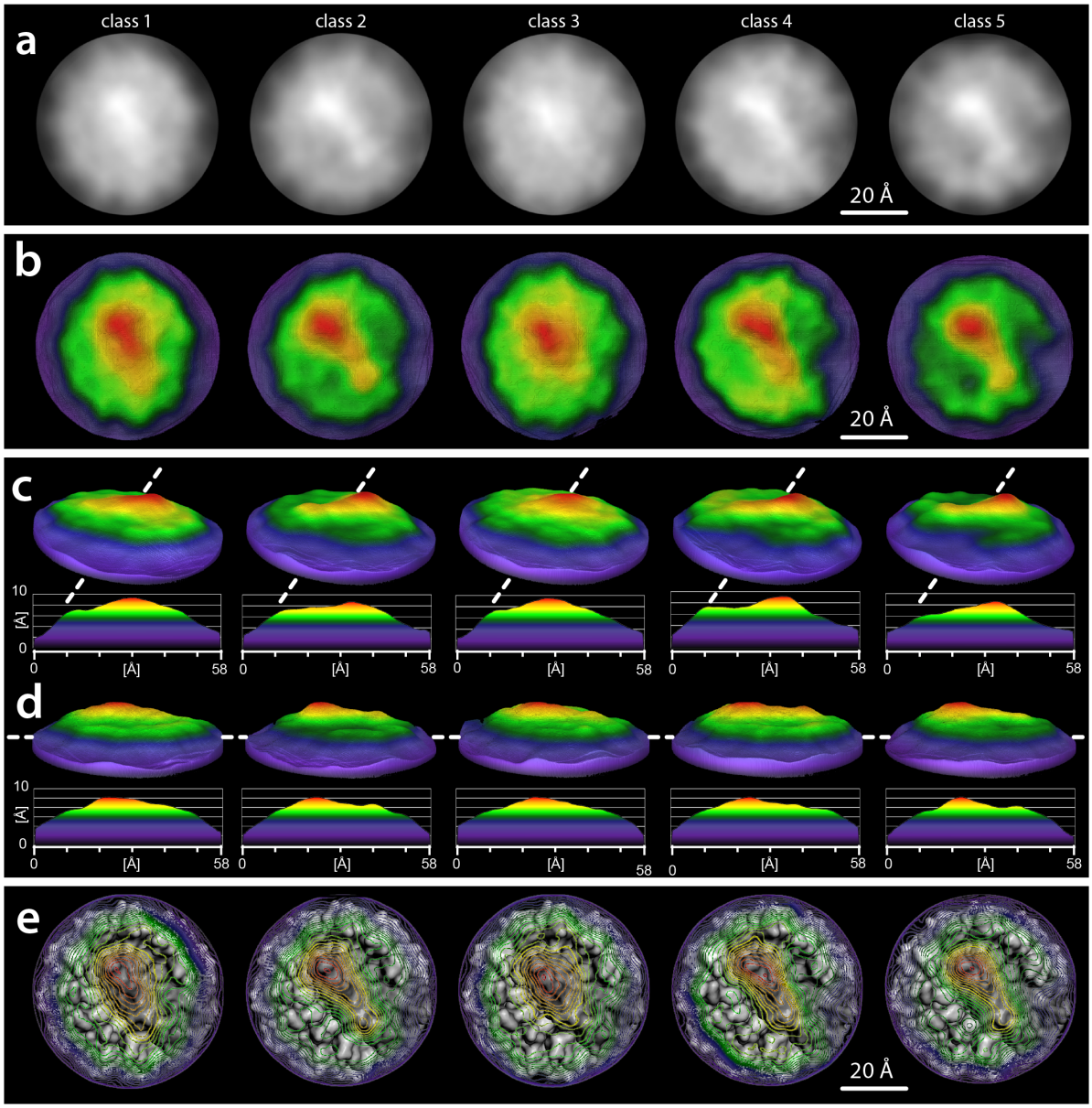

Supplementary Figure 7. Molecular-resolution AFM imaging of the *A. woodii* c-ring. (**a**) Topograph of *A. woodii* c-rings embedded in a lipid membrane (adapted from Fritz *et al*., *FEBS J.* **275**, 1999-2007 (2008), with kind permission from John Wiley and Sons, license number 3317651405161). (**b**) Class-averages representing five distinct conformations of the periplasmic face of the c-ring. Classes 1 through 5 contain 51, 60, 51, 46 and 52 particles, respectively. (**b**) Color-coded representations of the data in the class-averages shown in (a), according to height above the membrane plane (maximal in red, minimal in purple). (**c, d**) Three-dimensional representations of the data in (c), viewed diagonally from two different perspectives, and cross-sections of the data along the planes indicated by dashed lines. (**e**) Overlay of the map in (c), contoured according to height, on the *A. woodii* c-ring crystal structure, represented by its molecular surface. The c_1 subunit is shown in gray, and the $c_{2/3}$ subunits in white.

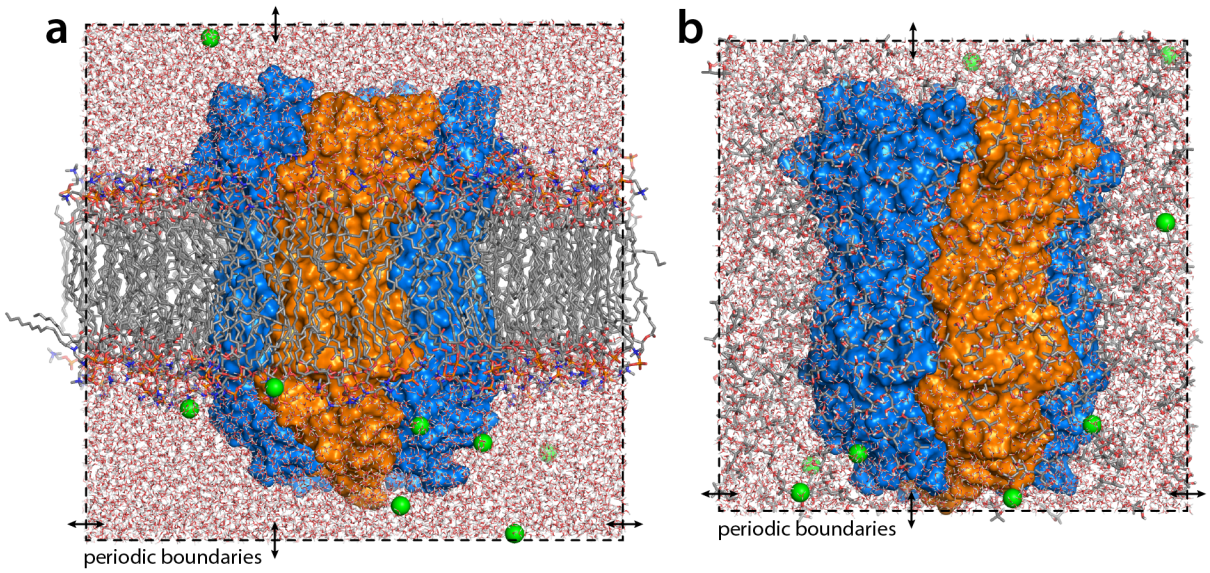

Supplementary Figure 8. Atomic systems used in molecular dynamics simulations of the *A. woodii* ring. The c-ring is represented as a molecular surface, with the V-type c_1 subunit in orange and the F-type single-hairpin $c_{2/3}$ subunits in blue. Na^+ ions are encompassed by the protein surface and are therefore not visible. (**a**) The c-ring embedded in a model lipid (POPC) bilayer. Carbon atoms are shown in gray, oxygen in red, nitrogen in blue and phosphorus in orange. Water molecules are shown in red/white. Hydrogen atoms in lipid molecules are omitted for clarity. Potassium counter-ions (green spheres) were added to neutralize the total charge of the system. (**b**) The c-ring immersed in a 30% (v/v) 2-methyl-2,4-pentanediol (MPD) buffer, after equilibration of the system (**Supplementary Fig. 9**). Atoms are colored as in panel (a).

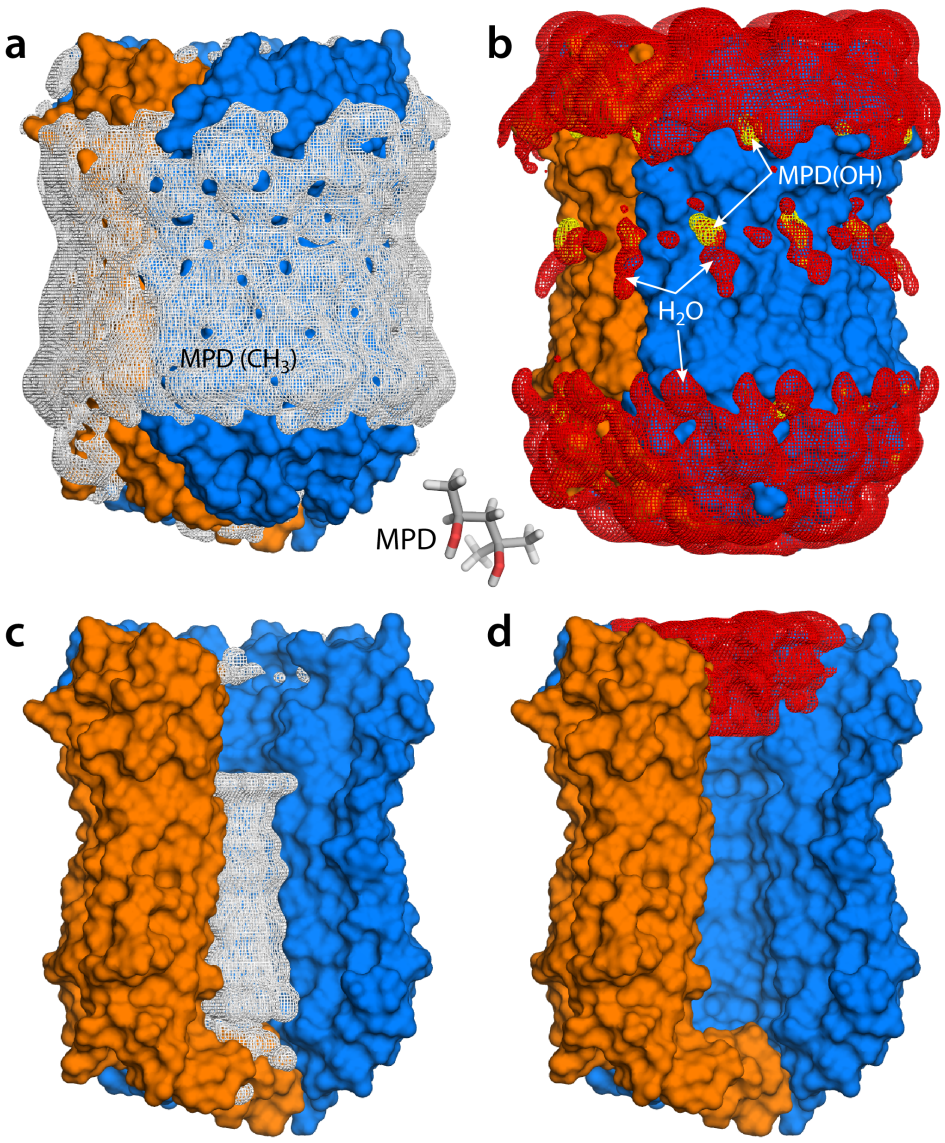

Supplementary Figure 9. Distribution of MPD and water molecules at the surface of the *A. woodii* c-ring. A solution buffer consisting of 30% (v/v) 2-methyl-2,4-pentanediol (MPD) in water was initially prepared by distributing MPD molecules uniformly across the simulation system in all dimensions, and adding water elsewhere. Within ~200 ns of simulation, a non-homogenous distribution emerges in which MPD molecules preferentially coat the hydrophobic surfaces of the c-ring, while polar regions on the protein surface, including the Na^+-binding sites, are hydrated. (**a**) Density map (white mesh) associated with MPD methyl groups in van-der-Waals contact (≤ 4.0 Å, excluding hydrogen atoms) anywhere on the c-ring surface, obtained by averaging instantaneous configurations over a 100-ns time-window in the simulation. The protein (solid surface) is colored as in **Fig. 1**, and viewed from the outside. (**b**) Same as panel (a), for water molecules (red mesh) or MPD hydroxyl groups (yellow mesh) in hydrogen-bonding range (≤ 3.0 Å, excluding hydrogen atoms) from the protein surface. (**c, d**) Same as panels (a) and (b), specifically for MPD and water contacts with side-chains facing the interior of the c-ring. The structure of an MPD molecule is shown to illustrate its amphiphilic character.

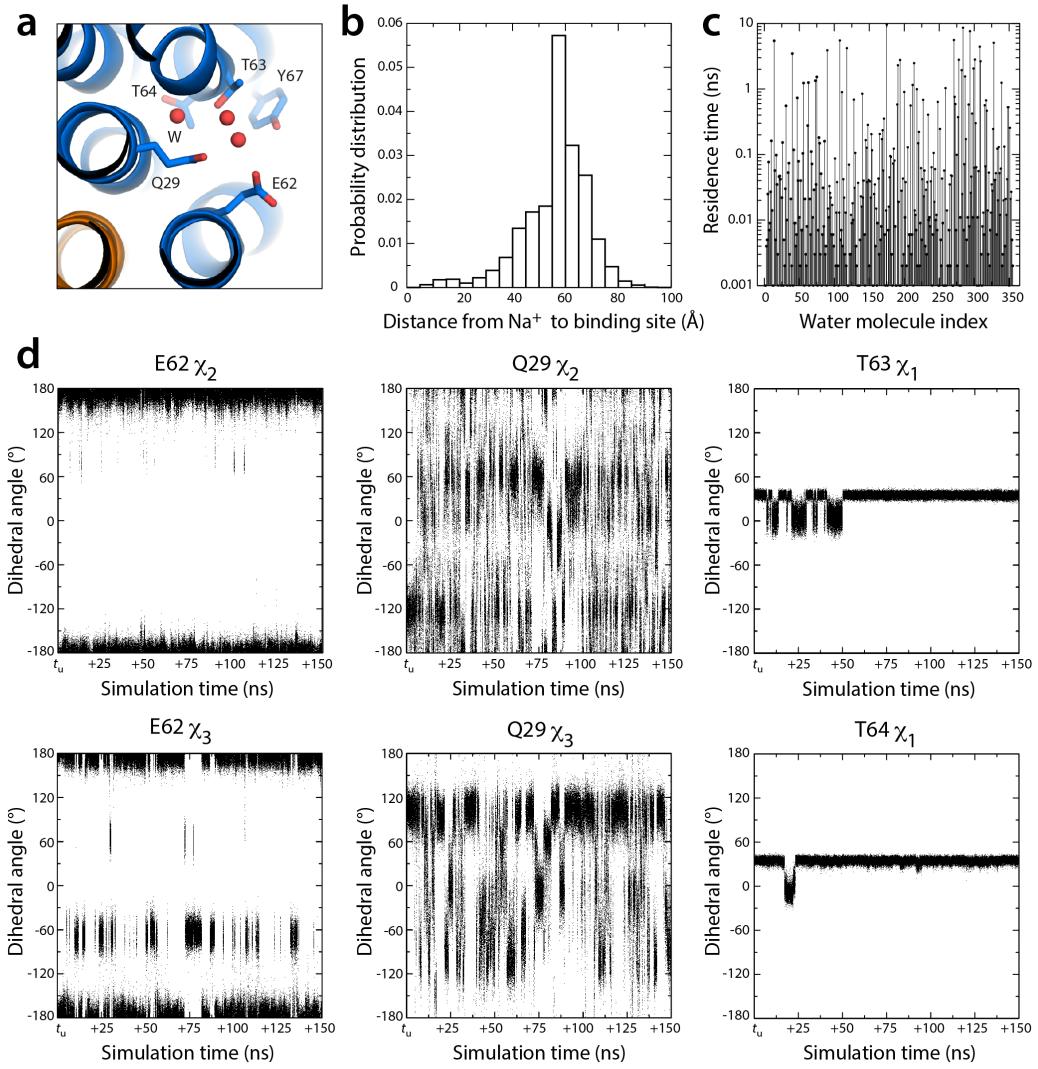

Supplementary Figure 10. Dynamics of the Na^+-binding site after spontaneous Na^+ release. (**a**) Snapshot of the Na^+-binding sites in one of the $c_{2/3}$ subunits immediately after Na^+ release into the solvent, at time t_u (**Fig. 4**). (**b**) Probability distribution of the distance between the released Na^+ and its binding site in the subsequent 150 ns of simulation, i.e. prior to Na^+ re-binding. (**c**) In this period, over 350 different water molecules bind transiently to the empty site – specifically hydrogen-bonding to Thr64, as seen in the Na^+-bound state (marked with "W" in panel (a)) – and subsequently return to the buffer. (**d**) The side-chains of Glu62, Gln29 and Thr63 also undergo multiple isomerizations in this time period. Altogether, this data demonstrates that the configurations of the site immediately after Na^+ release and immediately before Na^+ re-binding are structurally uncorrelated.

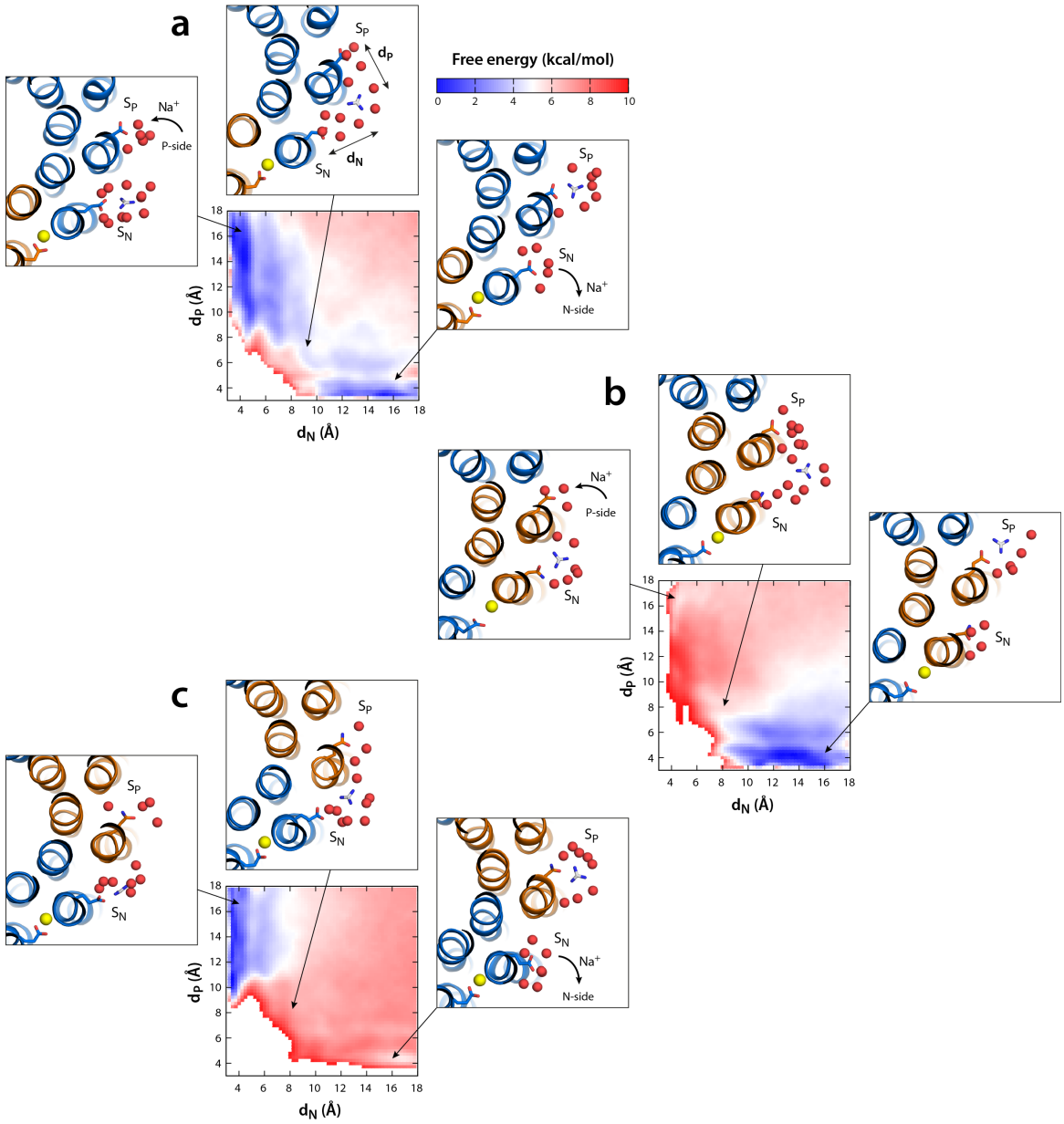

Supplementary Figure 11. Energetics of exchange of sequential subunit-a/subunit-c interactions in the rotary cycle of the *A. woodii* c-ring. The micro-environment of the c-ring ion-binding sites (blue and orange cartoons) at the subunit-a interface was simulated with an amphiphilic buffer consisting of MPD and water (not shown for clarity). A conserved Arg in subunit-a is mimicked with a GND^+ ion (gray/blue sticks). (**a**) GND^+ exchange between two unlocked Glu side-chains (blue sticks) in adjacent Na^+-binding sites, after Na^+ release from the S_N site, and prior to Na^+ loading to the S_P site. The figure shows representative simulation snapshots of the two end-point states in the exchange, and of the transition state in between. Note the GND^+ ion and the Glu carboxylate groups are always hydrated (red spheres). The calculated free energy of the exchange, in terms of the distance of the GND^+ ion to the S_P and S_N sites (d_P and d_N), is also shown. This 2D projection was reduced to the 1D profiles shown in **Fig. 8** by integration. (**b**) Exchange between the unlocked Gln side-chain in the c_1 subunit (orange sticks) and the Glu side-chain in the adjacent Na^+ site, counter-clockwise. (**c**) Exchange between the unlocked Gln side-chain in the c_1 subunit and the Glu side-chain in the adjacent Na^+ site, clockwise.

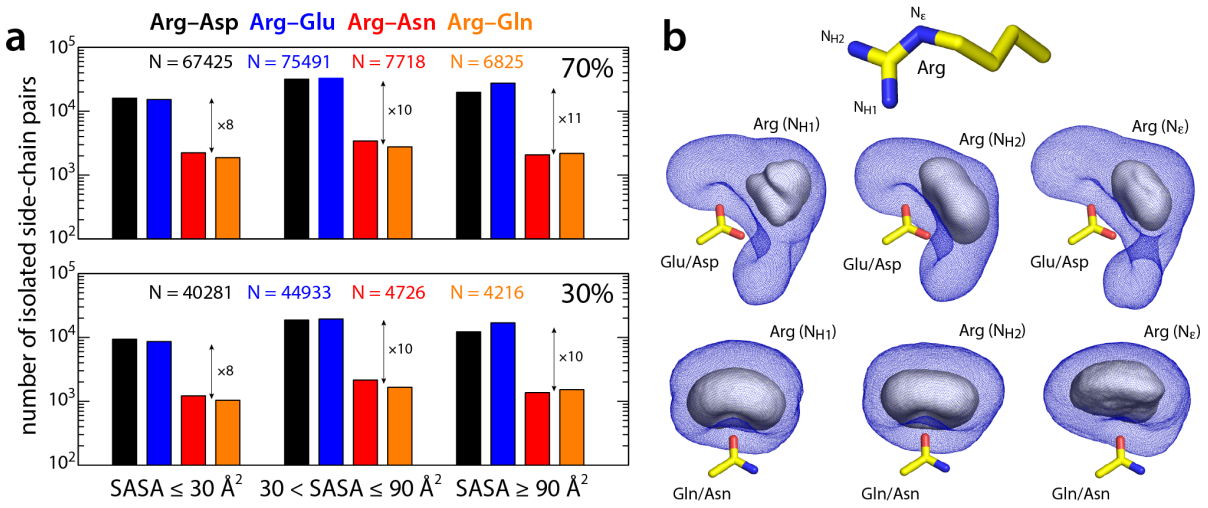

Supplementary Figure 12. Frequency and typical geometry of direct side-chain interactions between arginine and aspartate, glutamate, asparagine or glutamine, in experimental structures in the Protein Data Bank. This statistical analysis is restricted to protein structures solved by X-ray diffraction at a resolution of 3.0 Å or better, excluding redundant homologues, according to either a 70% or 30% sequence-identity cut-off. Protein-nucleic acid complexes were also excluded from this data set. (**a**) Number of isolated side-chain pairs (i.e. without other concurrent interaction partners) in each case, as a function of the combined solvent-accessible surface area of the interacting chemical groups (e.g. CN_3:COO). The total counts are also provided for each sequence-identity cut-off. Approximate ratios between ionic (Glu/Asp) and non-ionic (Gln/Asn) interactions are indicated. This analysis reveals that non-ionic (i.e. with Gln or Asn) interactions are only 8-10 times less frequent than ionic (Glu/Asp) interactions, i.e. a statistical energy difference of only ~ 2 kcal/mol. A cut-off distance of 3.0 Å between donor and acceptor was used to identify hydrogen-bonds. Only isolated side-chain pairs were considered in this analysis; pairs in which either side-chain interacts with additional protein groups were excluded. The solvent accessible surface area (SASA) of each of the side-chain pairs identified was calculated in the context of the complete protein. The atoms used in the SASA calculation are the four terminal atoms in each of the side-chains (excluding hydrogen atoms). The radius of the probe used to calculate the surface was 1.4 Å. (**b**) Geometry of the ionic and non-ionic side-chain pairs analyzed in (a). The atomic structures of all pairs identified in the PDB with 70% sequence-identity cut-off were overlaid optimizing the fit of the carboxylate/carboxamide group in the Asp/Glu/Asn/Gln side-chains. Density maps (blue mesh, white surface) were then computed based on the coordinates of each of the nitrogen atoms in the guanidinium group of the arginine side-chains. The data shows that the most probable geometry (white surface) of the ionic pairs is the so-called bi-dentate configuration, whereby the arginine donates two simultaneous hydrogen-bonds to the Asp/Glu carboxyl group. The non-ionic pairs, by contrast, are formed via a single hydrogen-bond donated to the carboxamide oxygen in the Gln/Asn side-chain.

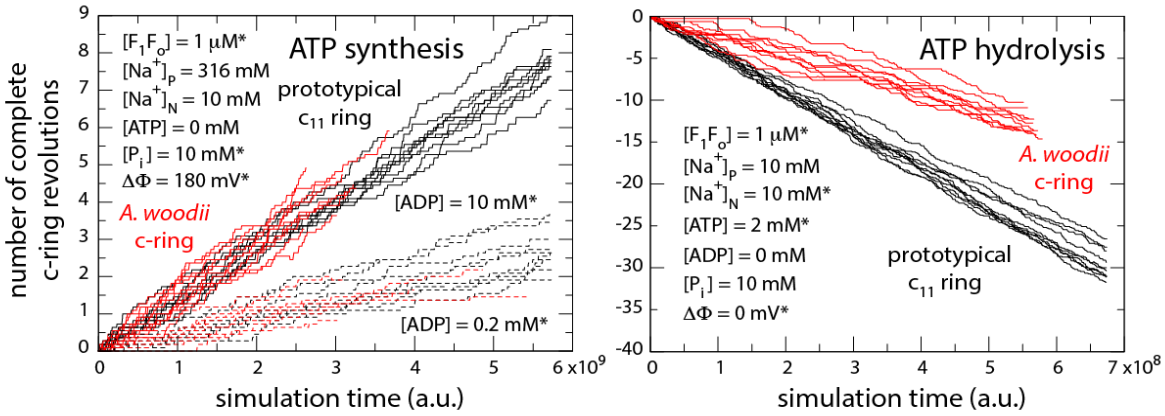

Supplementary Figure 13. Simulated rotational trajectories of the *A. woodii* F_1F_o-ATP synthase, relative to an analogous enzyme with a prototypical c_{11} ring. The trajectories were computed with kinetic-Monte Carlo simulations (Methods), under the conditions specified. Ten representative trajectories are shown in each case. The data shown in **Fig. 9d** reflect averages over 100 trajectories. The time-traces shown depict only transitions between rotational states – sub-states within those states are omitted for clarity. Counter-clockwise transitions are counted as positive; clockwise as negative. The concentration conditions specified are those set initially; those marked with (*) are kept constant, while all other are variable, although in the course of these simulations these do not change significantly. In longer simulations, however, significant changes would occur as equilibrium is reached (**Fig. 9bc**). At equilibrium, the number of counter-clockwise and clockwise revolutions cancel each other, on average (not shown). As the plot shows, the impact of the c_1 subunit in the *A. woodii* c-ring on the rotation rate is much smaller in the synthesis mode than in the hydrolysis mode. This result can be rationalized on the basis of the individual transitions rates that define the kinetic model (Methods). In both synthesis and hydrolysis, the slowest transitions are those associated with the rotational stepping of the c-ring (as opposed to e.g. Na^+ unbinding or the exchange between subunit-a/subunit-c ion-pair interactions). However, in ATP synthesis conditions the rate of these transitions is several orders of magnitude slower, because they are uphill in energy and because they require both ADP and P_i (**Methods, equation 10**); by contrast, the rotational transitions in ATP hydrolysis conditions are downhill and require ATP only (**Methods, equation 11**). Although in both cases the c_1 subunit imposes an additional kinetic barrier in the rotary cycle, not present in the prototypical c_{11} ring (**Fig. 9a**), the magnitude of this effect relative to the actual limiting rate in the cycle is much smaller in synthesis than it is in hydrolysis.

Supplementary Table 1.
Diffraction data collection and model refinement statistics

Data processing	
Wavelength (Å)	0.8726
Space group	$P4_32_12$
Cell dimensions	
a, b, c (Å)	121.2, 121.2, 150.6
α, β, γ (°)	90, 90, 90
Solvent content (%)	59.5
Resolution (Å)	47.2 - 2.1 (2.2-2.1)[a]
Number of observed reflections	1,083,343 (137,704)[a]
Number of unique reflections	65,395 (8,341)[a]
Redundancy	16.57 (16.51)[a]
Completeness (%)	99.3 (98.8)[a]
$R_{mergd\text{-}F}$ (%)[(b)]	14.3 (103.5)[a]
I/σ_I	18.08 (1.58)[a]

Refinement statistics	
Resolution (Å)	47.2 - 2.1
R_{work} / R_{free} (%)	18.18 / 21.98
Number of atoms	7,053
Protein	6,470
Ligands	408
Water	164
Ions	11
B-factors	59.2
Protein	55.0
Solvent	62.7
R.m.s deviations	
Bond length (Å)	0.007
Bond angles (°)	0.936

[(a)] Values in parenthesis are for the highest resolution shell. Inclusion of data up to 2.1 Å resolution resulted in noticeable improvements in the electron density, despite the high vale of $R_{mergd\text{-}F}$.

[(b)] $R_{\text{merdg-F}} = \sum_{hkl}\sqrt{\frac{n}{n-1}}\sum_{j=1}^{n}\left|F_{hkl,j} - \langle F_{hkl}\rangle\right| \Big/ \sum_{hkl}\sum_{j=1}^{n} F_{hkl,j}$

Supplementary Table 2. Coordination geometry in the Na^+ and water binding sites in the crystal structure of the *A. woodii* c-ring.

Na^+ sites in $c_{2/3}/c_{2/3}$, $c_{2/3}/c_1$ and $c_1/c_{2/3}$ interfaces		
From	To	Distance [Å][a]
Na^+	Gln29/46 $O\varepsilon_1$	2.29 ± 0.06
Na^+	Val60/160 O	2.36 ± 0.08
Na^+	Glu62/79 $O\varepsilon_2$	2.41 ± 0.05
Na^+	Thr63/163 Oγ	2.32 ± 0.06
Na^+	Water O	2.36 ± 0.13
Water O	Ala61/161 O	2.74 ± 0.22
Water O	Thr64/164 Oγ	2.69 ± 0.09
Glu62/79 $O\varepsilon_2$	Gln29/46 $N\varepsilon_2$	2.81 ± 0.10
Glu62/79 $O\varepsilon_1$	Tyr67/167 O_H	2.80 ± 0.18
Glu62/79 $O\varepsilon_1$	Thr63/163 Oγ	2.66 ± 0.15
Water site within subunit c_1		
From	To	Distance [Å]
Water O	Ala78 O	2.85
Water O	Ser81 Oγ	2.68
Water O	Gln129 Oε	2.64
Gln162 Oε	Gln129 Nε	2.68
Gln162 Nε	Thr80 Oγ	3.23
Thr80 $O\varepsilon_1$	Val77 O	2.97

[(a)] The values shown are averages, with the corresponding standard deviations, over the 10 binding sites in one c-ring. The structural refinement was carried out without non-crystallographic symmetry restraints, either on the Na^+ or the bound water molecules.